Williams Richard (Orcid ID: 0000-0001-6067-1947)

Three-dimensional reconstruction of fluvial surface sedimentology and topography using personal mobile laser scanning

Richard David Williams[1], Marie-Lou Lamy[2], Georgios Maniatis[3], Eilidh Stott[1]

[1]School of Geographical and Earth Sciences, University of Glasgow, Glasgow, United Kingdom

[2]Ecole Nationale des Sciences Géographiques (ENSG), Paris, France

[3]School of Environment and Technology, University of Brighton, United Kingdom

Submission to ESPL: Letters to ESEX (methodological developments)

Abstract

High resolution quantification of fluvial topography has been enabled by a number of geomatics technologies. Hyperscale surveys with spatial extents of <1 km^2 have been widely demonstrated by means of Terrestrial Laser Scanning (TLS) and Structure from Motion (SfM) photogrammetry. Recent advances in the development and integration of Global Navigation Satellite System (GNSS), Inertial Measurement Unit (IMU) and lightweight laser scanning technologies are now resulting in the emergence of personal mobile laser scanners (MLS) that have the potential to increase data acquisition and processing rates by 1-2 orders of magnitude compared to TLS/SfM, and thus challenge the recent dominance of these technologies. This investigation compares a personal MLS survey using a Leica Pegasus Backpack that integrates Velodyne Puck VLP-16 sensors, and a multi-station static TLS survey using a Riegl VZ-1000 scanner, to produce Digital Elevation Models (DEMs) and surface sedimentology maps. The assessment is undertaken on a 500 m long reach of the braided River Feshie. Comparison to 107 independent Real Time Kinematic (RTK)-GNSS check points resulted in similar Mean Error (ME) and Standard Deviation Error (SDE) for TLS (ME = -0.025 m; SDE = 0.038 m) and personal MLS (ME = -0.014 m; SDE = 0.019 m). Direct cloud-to-cloud (C2C) comparison between a sample of TLS and personal MLS observations (2.8 million points) revealed that C2C distances follows

This article has been accepted for publication and undergone full peer review but has not been through the copyediting, typesetting, pagination and proofreading process which may lead to differences between this version and the Version of Record. Please cite this article as doi: 10.1002/esp.4747

a sharply decreasing Burr distribution (a=2.35 b=3.19, rate parameter s = 9.53). Empirical relationships between sub-metre topographic variability and median sediment grain size (10-100 mm) demonstrate that surface roughness from personal MLS can be used to map median grain size. Differences between TLS and personal MLS empirical relationships suggest such relationships are dependent on survey technique. Personal MLS offers distinct logistical advantages over SfM photogrammetry and TLS for particular survey situations and is likely to become a widely applied technique.

Keywords

Personal mobile laser scanning, terrestrial laser scanning, topography, morphodynamics, sedimentology.

1. Introduction

Quantification of the Earth's surface topography has been transformed by a number of innovative geomatics technologies such as Real Time Kinematic Global Navigation Satellite System (RTK-GNSS) surveying, airborne Light Detection and Ranging (LiDAR), terrestrial laser scanning (TLS), multibeam SONAR, and Structure-from-Motion (SfM) with multi-view stereo (MVS) hereafter together referred to as SfM photogrammetry (Carrivick and Smith, 2018). These technologies are enabling the acquisition of topographic data with unprecedented spatial resolution (Passalacqua et al., 2015). Such datasets have a variety of uses in geomorphology, including landform mapping and classification (Pasternack et al., 2018, Jones et al., 2007, Demarchi et al., 2016, Carbonneau et al., 2012), topographic change detection (Wheaton et al., 2010, Tamminga et al., 2015), surface grain size characterisation using point clouds derived from TLS (Brasington et al., 2012, Heritage and Milan, 2009, Hodge et al., 2009a) and SfM photogrammetry (Pearson et al., 2017, Westoby et al., 2015, Vázquez-Tarrío et al., 2017), hydro- and morpho-dynamic modelling (Williams et al., 2016, Williams et al., 2013, Kasprak et al., 2018) and vegetation mapping (Manners et al., 2013, Brodu and Lague, 2012, Jalonen et al., 2014). Recently, a new generation of lightweight LiDAR sensors have emerged. These sensors are sufficiently light to mount on personal platforms (e.g. backpacks) but have lower ranging and positional accuracies than heavier, high-end terrestrial laser scanners. For example, Velodyne's Puck VLP-16 lightweight sensor has a mass of 830 g and a manufacturer quoted accuracy of 30 mm at the sensor's maximum range of 100 m, whilst Leica's P40 high-end TLS has a maximum range of 270 m and a three-dimensional (3D) position accuracy of 6 mm at 100 m range. A number of personal Mobile Laser Scanning (MLS) systems, also known as Personal Mobile Terrestrial Systems (PMTS; Campos et al., 2018) are now emerging that integrate lightweight laser scanners with an Inertial Measurement Unit (IMU) and GNSS to enable positioning of the laser scanner's position and attitude.

Such systems potentially offer considerable benefits over alternative topographic measurement technologies for the derivation of high-resolution models of surface sedimentology and topography but have yet to be verified at a spatial scale typical for geomorphic applications.

Topographic surveys in fluvial geomorphology have, in particular, been transformed by two technologies; TLS from tripod or equivalent static setups (Milan et al., 2007, Lague et al., 2013, Williams et al., 2014) and SfM photogrammetry (James and Robson, 2012, Westoby et al., 2012, Fonstad et al., 2013, Smith et al., 2015). The accuracy of TLS and SfM for generating georeferenced point clouds that can be used to produce Digital Elevation Models (DEMs) and maps of surface sedimentology are now well established. Each of these technologies does, however, have limitations. TLS is associated with labour intensive equipment set up, which can demand multiple field days for surveys with longitudinal lengths of > 1 km across complex relief (e.g. Williams et al., 2014) if valley side vantage points are not available for long range scanning of valley topography. SfM photogrammetry is being widely applied in geomorphology but significant challenges are associated with: (i) acquiring imagery from Unmanned Aerial Vehicles (UAVs; Woodget et al., 2017) due to weather conditions and flight permissions; (ii) the computational resources required for data processing for spatially extensive surveys (>1 km longitudinal length); (iii) systematic errors (James and Robson, 2014; Eltner et al., 2016); and (iv) laying out and recovering ground control points (James et al., 2017). Although direct georeferencing of imagery (Hamshaw et al., 2017) may overcome this latter challenge. The emergence of personal MLS potentially offers an alternative survey platform that addresses some of the limitations associated with TLS and SfM in particular survey situations.

Hardware and software developments in personal MLS have primarily been driven for applications in indoor mapping for Building Information Systems (BIM; Jung et al., 2015; Lauterbach et al., 2015) and in forestry inventories to characterise tree size and shape. With respect to the latter, a high-end backpack-mounted laser scanning system has been shown to be capable of delivering equivalent estimates of tree attributes, such as biomass, height, and stem location, curvature and volume, to TLS for forests where the tree structure is simple (Liang et al., 2014; Rönnholm et al., 2016; Liang et al., 2018). Examples of high-end systems being used to acquire topographic data for geomorphological investigations are now emerging (e.g. Kukko et al., 2012; Flener et al., 2013; Calle et al., 2015; Lotsari et al., 2015; Brooks et al., 2017; Lotsari et al., 2018). High-end mobile systems have also been applied to map surface sedimentology, for example Wang et al. (2013) model sediment grain size at a 2 m^2 patch, by segmenting a Digital Surface Model (DSM) and then fitting ellipsoid models to the personal MLS points associated with individual particles to estimate particle size, sphericity and orientation. In comparison, the evaluation of lightweight laser scanners has received less attention, although a

personal system with a Velodyne VLP16 laser scanner has been demonstrated to estimate tree stem diameter (Overland et al., 2017). In the field of geomorphology, Glennie (2013) compared a TLS survey of a bare earth environment with a personal MLS that incorporated a Velodyne HDL-32E laser scanner. Results indicated that the personal MLS point cloud target residuals were within 0.01-0.02 m of TLS observations. However, the configuration of the scanner within the backpack system meant that only a 4 m wide swath of data were acquired and evaluated. To date, personal MLS systems that have incorporated both high-end and lightweight laser scanners have tended to be fabricated using multiple independent systems (e.g. laser scanner, IMU, GNSS), but integrated, commercial, "out of the box" systems are now emerging. Such systems offer transformative potential for geoscientists who don't have the geomatics expertise to build systems from individual components and instead want to focus upon deploying geomatics technologies to investigate geomorphological questions. However, to our knowledge, there are no integrated investigations that verify the errors of personal MLS for topographic and sedimentological applications in fluvial geomorphology.

This aim of this paper is to evaluate the performance of a personal MLS system that integrates a low-cost, lightweight laser scanner in a topographically complex environment, at the reach scale. The first objective is to assess planimetric and vertical accuracy. The second objective is to evaluate whether observations can be used to estimate surface grain size. Our motivation is to consider whether lightweight personal MLS offers comparable accuracy to other established survey techniques used by geomorphologists, namely TLS and SfM photogrammetry, which are currently the most widely used approaches to acquire datasets with sufficient high point densities to map grain size. Investigation of our second objective is particularly important because the manufacturer quoted accuracy of lightweight scanners is close to the minimum in the range of standard deviation of elevations that are used to map grain size in gravel-bed river environments. Regarding personal MLS performance, we contrast the characteristics of this system to SfM photogrammetry and TLS, and we also outline a list of considerations for undertaking topographic surveys using personal MLS.

2. Methodology

2.1. Study Site

A braided reach of the gravel-bed, River Feshie, Scotland (Figure 1a), was chosen due to its complex relief and spatially variable grain size, thus providing a stringent test environment. The Feshie drains a catchment of 231 km^2 that is underlain by Moine schists together with a small portion of granite which underlies higher land in the north-east (Werritty and McEwen, 1993). These two rock types dominate the coarse proportion of the river's sedimentary load, with typical D_{50} values for schistose

material being between 50 and 110 mm (Brasington et al., 2012; Figure 1b). The 500 x 250 m study site is located upstream from Feshie Lodge; this area is the most active and dynamic braided reach along the Feshie and has been subject to multiple investigations that have developed and applied novel geomorphological techniques (e.g. Wheaton et al., 2010, Brasington et al., 2003, Hodge et al., 2009b, Wheaton et al., 2013). The study site was last glaciated during the Late Devensian and went through an episode of deglaciation ~13000 BP (Gilvear et al., 2000). The remnants of this glaciation can now be observed as large fluvio-glacial outwash terraces which comprise the flanks of the wide valley. Steep channel and hillslope gradients, coupled with high runoff, a flashy flow regime and substantial coarse sediment supply (Rumsby et al., 2008) has resulted in a morphologically dynamic braided channel. A number of bars on the braidplain are vegetated, with a combination of grasses, sedges, and heather, and Scots Pine (*Pinus sylvestris*) and Silver Birch (*Betula pendula*) saplings that are growing in response to a reduction in deer numbers (MacDonald, 2016).

2.2. Personal Mobile Laser Scanning

A Leica Pegasus backpack system (Figure 1d and 1e) was used to scan the study site (Figure 1c). This backpack integrates an inertial navigation system, comprised of a Novatel 700 series GNSS receiver, a 125 Hz Inertial Measurement Unit (IMU), and two Velodyne Puck VLP-16 scanners. Each scanner has a range of 100 m, 16 laser channels with a wavelength of 903 nm, a 360˚ field of view around the 103 mm diameter cylindrical scanner's planimetric axis and a ±15˚ field of view across the scanner's vertical axis. The two VLP-16 scanners are mounted on the front and top of the backpack, enabling approximately vertical and planimetric scanning as the backpack is carried across terrain. All lasers on each scanner are fired and recharged every 55.296 µs, yielding a scan rate of c. 300,000 points/s. Multiple survey lines are thus profiled at the same time. At the start and end of the survey, the backpack was positioned on the ground to acquire static GNSS observations for a minimum of five minutes. During the survey, the backpack system was worn by an operator who navigated the complex braided river terrain at a steady walking pace (Figure 1e) in a sequence of loops, totalling a length of 3407 m (as shown in red in Figure 1c). The observations took one person approximately one hour to acquire. The scanning trajectory was determined to ensure the scanners had line of sight across all areas of the complex terrain. The backpack system has previously been demonstrated for the application of mapping flood inundation (Sayama et al., 2019).

Novatel Inertial Explorer software (Hexagon, 2017) was used to post-process backpack GNSS and IMU observations, and RINEX data from the nearest OSNet station, to calculate the backpack's trajectory. Leica Pegasus Automatic Processing software (Leica Geosystems, 2017b) was then used to generate a 3D point cloud from observations acquired within a range of 0.5 – 50 m from the backpack. The

resulting point cloud was subsequently decimated to 0.02 m and edited, using Cyclone software (Leica Geosystems, 2019a), to manually clip out TLS targets, large trees and tree saplings. Finally, the edited point cloud was processed using TopCAT (Brasington et al., 2012) software to calculate statistical summaries of topographic variability at resolutions of 0.1, 1 and 2 m spatial resolution. These summaries included the minimum elevation, z_{min}, and the detrended standard deviation of the elevation distribution, σ_z, in each grid cell. From the 0.1 m resolution analysis, z_{min} was used to produce a DEM. From the 1 and 2 m resolution analysis, σ_z was used to develop an empirical relationship with sampled surface grain size. Two resolutions were required due to the use of 1 m^2 and 4 m^2 sample grids (see Section 2.4).

2.3. Topographic verification: Terrestrial Laser Scanning and RTK-GNSS

A base station, set up at a field adjacent to the study site, was observed in GNSS static mode for eight hours with Leica GS10. Post-processing with RINEX data from the nearest Ordnance Survey (OS) Net station (BRAE) was performed to calculate the base station's coordinates in Ordnance Survey Great Britain (OSGB36(15)). The study site was scanned using a long-range Riegl VZ-1000 terrestrial laser scanner, using a similar survey protocol to Brasington et al. (2012). The VZ-1000 was levelled on a tripod at 26 scanning stations (as shown in orange circles on Figure 1c) to acquire overlapping scans that enabled complete spatial coverage of the study site. A network of 12 highly reflective, flat, six inch circular targets were set up across the study site in a configuration that enabled each scan station to include at least three targets that were common with another scan station. Each target was observed for at least 30 minutes in GNSS-static mode. The TLS and GNSS observations took a team of two people a total of four days to acquire. The targets' coordinates were calculated via post-processing of the GNSS raw observations relative to the BRAE base. RiScan software (Riegl, 2017) was used to register the scans using the positions of the 12 targets. The 3D standard deviation of registration residuals across the 12 targets was 0.024 m (n = 119). Standard deviations were similar across the X, Y and Z planes; respectively 0.010, 0.007 and 0.011 m. The TLS point cloud was subsequently decimated, manually edited and processed using TopCAT using the same procedure that was applied to the backpack observations.

Two additional datasets were acquired to further assess the personal MLS outputs. First, six of the targets that were positioned within the study site for the TLS survey were also scanned during the personal MLS survey. No additional effort was made to guide the trajectory of the personal MLS survey to be closer to the targets. The range of distances between the six targets and the nearest personal MLS trajectory was 1.3-15.3 m. Secondly, 107 observations over dry terrain were acquired in RTK GNSS mode using Leica GS10, with its antenna mounted on a pole. The mean standard deviation point

quality for the 107 RTK-GNSS points was 0.005±0.001 m, 0.008±0.001 m and 0.009±0.001 m for planimetric, vertical and 3D components respectively.

2.4. Surface grain size sampling

Fourteen patches of sediment were sampled using a 100 clast grid count technique, immediately after the backpack and TLS surveys. This technique is equivalent to the Wolman (1954) pebble count approach. The a-, b- and c-axes of clasts were measured at evenly spaced intervals across each grid square. Grid spaces were at least as large as the D_{max} particle size within each sample (Bunte and Abt, 2001), resulting in either 1 or 4 m^2 grids.

2.5. Topographic and grain size mapping comparisons

To assess the vertical and planimetric accuracy of the personal mobile laser scanner, the positions of six targets were extracted from the personal MLS-borne point cloud and compared to their GNSS-static surveyed positions. Positions were extracted from the point cloud by choosing the point closest to the centre of each target. Since vertical error is usually more significant for surveys of geomorphologically complex environments than planimetric error, the two further accuracy assessments focused on vertical error. First, the coordinates of 100 RTK-GNSS surveyed points were compared to 0.1 m spatial resolution personal MLS and TLS DEMs, using the Extract Values to Points tool in ArcMap software (ESRI, 2014). Second, a direct MLS to TLS point cloud comparison was undertaken from a sample of the 0.02 m MLS and TLS edited point clouds. Figure 1c shows the extent of ten sample areas which were chosen as they represent areas of aerially exposed gravel with minimal alive or dead (e.g. deposited clumps of heather from bank erosion) vegetation, each with an area of c. 100 m^2 and incorporating 2.7 million point observations in total. The MLS and TLS observations for each area were compared using the cloud-to-cloud (C2C) distances tool of CloudCompare (Lague et al., 2013). The calculation was performed using the default settings since the high point density (0.02 m) of the personal MLS and TLS clouds allowed for the consistent application of the nearest neighbour algorithm (Lague et al., 2013; Jafari et al., 2017). The C2C distances were subsequently treated statistically using the *fitdisrt* library (Delignette-Muller et al., 2015) of R software (R Core Team, 2013).

To evaluate whether point cloud data can be used to estimate surface grain size, D_{50} particle diameters were calculated from the physical grain size samples (Section 2.4). Detrended standard deviation of elevations, σ_z were extracted at the location of each physical sample from the TopCAT (Brasington et al., 2012) personal MLS and TLS results. Linear regression was then used to examine the relationship between D_{50} and σ_z, thus using an established procedure for comparing single roughness values

between patches and point clouds (Westoby et al., 2015, Pearson et al., 2017; Neverman et al., 2019; Reid et al., 2019).

3. Results

3.1. Topography

Figure 2 shows the personal MLS-generated DEM of 0.1 m spatial resolution. The topographic detail of diagonal bar complexes is evident, with chute channels dissecting bars particularly clear (Figures 2b and c). Qualitatively, from the DEM visualisation in this figure, it is evident that the DEM is rich in topographic detail. The density of the personal MLS observations shows a considerably different pattern to the TLS observations (Figure 3), caused by the different scanning positions associated with each platform. For both surveys, areas of low density are associated with occlusion due to vegetation. Many backpack-generated trajectories close to each other are observed at the north part of the study site. These resulted in denser point clouds and higher spatial resolution in comparison to TLS-borne point clouds.

When performing a quantitative assessment of the vertical and planimetric accuracy of the personal MLS observations and derived DEM some assumptions must be made. Here, it is assumed that the GNSS derived positional errors associated with targets and ground observations are small relative to the accuracy of georeferenced survey points in the personal MLS and TLS point clouds. Comparisons between the six target positions and the personal MLS point cloud (Table 1) show that there is a greater bias in elevation, with a Mean Error (ME_z) of 0.051 m, rather than in planimetric directions (ME_x = -0.025 m, ME_y = -0.014 m). The Standard Deviation Error (SDE) is comparable in all three dimensions, ranging from 0.019 to 0.038 m. The 3D SDE (0.026 m) is similar to the 3D SDE of registration residuals across the 12 TLS targets (0.024 m; Section 2.3) . Although the targets are useful in evaluating the errors in each dimension, the sample size is small (n = 6). Table 2 shows elevation errors for 107 RTK-GNSS check points that were distributed across dry topography. Across all the error metrics, the 0.1 m DEM derived from personal MLS was characterised by lower error than the TLS DEM. Since the vertical absolute accuracy delivered from RTK-GNSS positioning was 0.008±0.001 m (Section 2.3), the personal MLS error is therefore approaching a value that is similar to the vertical accuracy of the RTK-GNSS check points.

The final component of the topography accuracy assessment was to compare directly the 0.02 m point clouds that were produced from personal MLS and TLS. The C2C distances follow a distinctively heavy tail Burr distribution (a=2.35 b=3.19, s = 9.53, Figure 4). For the fitting of the Burr distribution, a maximum likelihood estimation approach was followed to compare four right tail candidate

distributions (Cullen and Frey diagram [Cullen and Frey, 1991], Figure S1. See supplementary material.); a Weibull, a gamma, a log-normal and a Burr. The Burr model had the highest log-likelihood value and the lowest Akaike's and Bayesian information criteria values (AIC and BIC, Table S1. See supplementary material.). It also preforms better in the graphical tests (Histogram fitting, Q-Q plot and P-P plot, Figure S2. See supplementary material.). The median personal MLS to TLS C2C distance relaxes at 0.076 m and the maximum is at 0.6 m. Values >0.18 m are outliers (Figure 4, boxplot), with the third quartile of the C2C distances relaxing at 0.095 m and the 0.95 probability estimate quartile equal to 0.14 m. The stability of the selected distribution was assessed with bootstrapping (Figure S3. See supplementary material.). Parameter a varies in a range = 0.04, parameter b in a range = 0.015 and s in a range = 0.08, indicating that the parameters are relatively stable for the scale of the measurements.

3.2. Grain size mapping

Figure 5 shows the relationship between particle D_{50} and detrended standard deviation of elevations obtained using personal MLS and TLS. Sediment samples (Figure 1b) were either moderately sorted or moderately well sorted, as classified using the Folk and Ward (1957) graphic method. Relationships between D_{50} and σ_z had different gradients and intercepts for the personal MLS and TLS observations. The strength of the linear relationships were, however, similar (R^2 of 0.79 and 0.73). For a given sample, σ_z values from the personal MLS observations were generally greater than σ_z values from the TLS point cloud. This difference is particularly evident for finer D_{50} samples; if samples for $D_{50} < 0.025$ m are considered, there is no positive linear relationship between σ_z from the personal MLS observations and D_{50}. The linear relationships were used to map surface grain size across the study site (Figure 6). Local grain sorting patterns are revealed by the maps that are derived from both personal MLS and TLS observations. The broad grain size patterns are similar for the four classes that are mapped but there is data source sensitivity around classification boundaries.

4. Discussion: an additional method for high-resolution topographic surveys

High-resolution DEMs provide fundamental data for geomorphological analyses and boundary data for hydro- and morpho-dynamic numerical modelling (Tarolli, 2014). Thus, the presented investigations have demonstrated that personal MLS can generate datasets of high spatial resolution, featuring similar vertical and planimetric accuracies to TLS. This investigation therefore demonstrates that personal MLS laser scanning is capable of generating observations that feature similar vertical and planimetric errors to TLS surveys. Results from distributed RTK-GNSS check points (n = 107; Table 2) indicate that vertical errors associated with a 0.1 m resolution DEM derived from personal MLS

observations were lower than those associated with an equivalent TLS product. However, data from targets (n = 6) indicated that 3D errors were greater for the personal MLS (Table 1) than the TLS observations. The direct comparison of the personal MLS and TLS observations (Figure 4) revealed a median difference of 0.07 m. The outliers for the C2C distances ranged from 0.18 to 0.53 m and were randomly distributed across the 10 sampled areas. It is likely that those high C2C distances were a combination of higher relative ranging errors from the MLS at short range. As well as the greater likelihood of the personal MLS sampling between individual clasts compared to the TLS. As this technique usually scanned the surface from a greater range and is therefore more likely to scan the tops of clasts due to an oblique view. When interpreting the C2C median difference of 0.07 m, the range of D_{50} values (50 to 100 mm for the study site; Section 2.1) should be taken into account. Overall, the differences between the personal MLS and TLS observations are likely to be caused by various parameters such as: (a) different laser scanner accuracies; (b) different lines of sight; (c) different point densities due to the differing nature of data acquisition from static stations and a moving trajectory; and (d) the registration process and filtering methods. Personal MLS surveys outperforms TLS surveys in acquiring observations with possibly fewer occlusions due to line of sight, because personal MLS can capture complex topography from numerous angles along a trajectory. Optimising the density of TLS stations to maintain line of sight across a surface with varying aspects can adversely affect TLS survey rates. Conversely, personal MLS can overcome the aforementioned limitation providing a considerably quick laser scanning acquisition. The lower errors associated with the personal MLS DEM (Table 2) may therefore be associated with the relative advantage of sampling along a trajectory.

Empirical relationships between surface roughness and median grain size indicate that there is too much noise in personal MLS observations to develop linear relationships for $D_{50} < 25$ mm. However, these personal MLS observations can be used to derive maps of surface sedimentology that are thresholded at intervals of 32, 64, 128, and 256 mm. The poor relationship for finer sediment is not surprising since the manufacturer quoted accuracy of the Velodyne's Puck VLP-16 is 30 mm at 100 m, which is less than the accuracy of the Riegl VZ-1000 scanner. The empirical relationship derived between D_{50} and σ_z for TLS during this investigation had a similar gradient but a poorer R^2 value compared to the relationship derived by Brasington et al. (2012) on the same river (their relationship was $D_{50} = 2.59\ \sigma_z + 0.012$; $R^2 = 0.917$; n = 12). This difference may be attributed to the effects of sorting which Pearson et al. (2017) identified as an important variable in determining the empirical relationship between D_{50} and σ_z. The linear regression model developed by Pearson et al. (2017) for moderately well sorted gravel sampled in the field had a similar R^2 value (0.710) to the TLS and personal MLS relationships derived in this study. The different empirical relationships for TLS and personal MLS are likely associated with the different laser scanner accuracies and sampling strategies

that characterise these survey technologies. Segmentation and modelling of all point observations potentially offers an approach for mapping grain sphericity and orientation, in addition to mapping grain size. Whilst such an approach has only been demonstrated at a patch scale (2 m^2) using personal MLS observations (Wang et al., 2013), the mapping of sphericity and orientation is potentially feasible from lightweight LiDAR sensors. Based on the findings reported here, for an approach to map grain sphericity and orientation the D50 > 50 mm should be taken into consideration. Moreover, for applications at a reach scale additional verification data are required to produce a sufficient computational analysis.

Personal MLS, using lightweight laser scanners such as the Velodyne Puck, is likely to become a common approach for undertaking topographic surveys. It could also complement existing geomatics technologies such as SfM photogrammetry and/or TLS when circumstances are appropriate. Table 3 compares personal MLS with these technologies in relation to deployment and data processing challenges, data products and costs. In recent years, SfM photogrammetry using images acquired from UAVs has become a remarkably popular topographic survey technique. However, obtaining permissions for flying UAVs is becoming more challenging in some countries, and the systematic errors that commonly arise during data processing can plague projects that aim to answer fundamental geomorphological questions. The direct laser observations obtained by personal MLS overcome these challenges, albeit for a higher hardware investment cost than is associated with SfM surveys. Compared to short-range TLS, personal MLS offer considerable time savings during both the survey and data processing stages of a survey. A limitation of personal MLS is that terrain must be navigable within the scanner range of the target area; soft ground, spiky and/or thick vegetation and deep water will thus pose challenges for this platform. Moreover, in common with TLS, personal MLS will need to be fused with direct or indirect bathymetric survey techniques (Williams et al., 2015, Williams et al., 2014, Legleiter, 2012) to acquire data in inundated areas. The issues that should be considered when planning, undertaking and processing personal MLS surveys are not dissimilar to those listed by Passalacqua et al. (2015) in their generic guidance for acquiring high-resolution topography. A personal MLS protocol does, however, require specific attention to be focused on planning a trajectory that has an appropriate acquisition perspective to cover all areas of interest.

Advances in laser scanner technologies, primarily driven by the development autonomous vehicle navigation systems (The Economist, 2016, Lee, 2018) has led to considerable technological progress and innovation in mobile laser scanning. Over the next decade, established survey hardware companies and new entrants are likely to offer a range of personal MLS platforms. In addition, the falling cost of RTK-GNSS, IMU and laser scanning hardware create opportunities for the fabrication of

bespoke systems. Together, these developments create opportunities for geomorphologists to add new tools to their armoury for quantifying the earth's surface at an unprecedented spatial and temporal resolution.

5. Conclusion

This investigation assessed the accuracy of personal MLS, using lightweight laser scanners, for deriving hyperscale DEMs of fluvial topography and surface sedimentology at the reach scale. An error analysis of a personal MLS point cloud and DEMs showed that vertical errors associated with personal MLS were comparable to those from TLS. The moving trajectory of personal MLS offers advantages over TLS in a topographically complex environment because it minimises problems associated with line of sight issues from TLS stations although the personal MLS trajectory needs to be appropriately planned to achieve this. Whilst lightweight laser scanners are inherently less accurate than high-end laser scanners, the acquisition of data whilst moving along a pathway during personal MLS is likely to enable a more complete representation of surface roughness as a greater proportion of a topographic surface is surveyed from a shorter range than is usually achieved from TLS stations. Results showed that it was feasible to map surface sedimentology using an empirically derived relationship between median grain size and surface roughness derived from personal MLS observations. The empirical relationship did, however, differ to that produced from TLS point cloud data, adding to the growing evidence that such relationships are dependent on both survey technique and sedimentological characteristics such as sorting. Personal MLS scanning using integrated scanning and positioning hardware, and associated data processing software, offers distinct advantages over SfM photogrammetry and TLS for some survey situations. It adds to the choice of methods that can be selected by geomorphologists when deciding upon the most appropriate technology, or suite of technologies, to acquire hyperscale data.

References

Bertin S, Friedrich H. 2016. Field application of close-range digital photogrammetry (CRDP) for grain-scale fluvial morphology studies. Earth Surface Processes and Landforms. 41 : 1358-1369. DOI: 10.1002/esp.3906

Brasington J, Langham J, Rumsby B. 2003. Methodological sensitivity of morphometric estimates of coarse fluvial sediment transport. Geomorphology. 53 : 299-316. DOI: 10.1016/S0169-555X(02)00320-3

Brasington J, Vericat D, Rychkov I. 2012. Modelling river bed morphology, roughness and surface sedimentology using high resolution terrestrial laser scanning. Water Resources Research. 48 : W11519. DOI: 10.1029/2012WR012223

Brodu N, Lague D. 2012. 3D terrestrial lidar data classification of complex natural scenes using a multi-scale dimensionality criterion: Applications in geomorphology. ISPRS Journal of Photogrammetry and Remote Sensing. 68 : 121-134. DOI: 10.1016/j.isprsjprs.2012.01.006

Brooks BA, Minson SE, Glennie CL, Nevitt JM, Dawson T, Rubin R, Ericksen TL, Lockner D, Hudnut K, Langenheim V, Lutz A, Mareschal M, Murray J, Schwartz D, Zaccone D. 2017. Buried shallow fault slip from the South Napa earthquake revealed by near-field geodesy. Science Advances. DOI: 3. 10.1126/sciadv.1700525

Bunte K, Abt SR. 2001. Sampling surface and subsurface particle-size distributions in wadable gravel- and cobble-bed streams for analyses in sediment transport, hydraulics, and streambed monitoring. Fort Collins, Colorado: U.S. Department of Agriculture, Forest Service, Rocky Mountain Research Station.

Calle, M., E. Lotsari E, A. Kukko A, P. Alho P, H. Kaartinen H, X. Rodriguez-Lloveras X, and G. Benito G. (2015),. Morphodynamics of an ephemeral gravel-bed stream combining Mobile Laser Scanner, hydraulic simulations and geomorphological indicators,. Zeitschrift für Geomorphologie, Supplementary Issues,. 59(3), : 33-57,. DOI: doi: 10.1127/zfg_suppl/2015/S-59196.

Campos, M. B., A. M. G. Tommaselli AMG, E. Honkavaara E, F. D. S. Prol FDS, H. Kaartinen H, A. El Issaoui A, and T. Hakala T. (2018),. A Backpack-Mounted Omnidirectional Camera with Off-the-Shelf Navigation Sensors for Mobile Terrestrial Mapping: Development and Forest Application,. Sensors,. 18(3), : 827. DOI: 10.3390/s18030827.

Carbonneau PE, Fonstad MA, Marcus WA, Dugdale SJ. 2012. Making riverscapes real. Geomorphology. 137 : 74-86. DOI: 10.1016/j.geomorph.2010.09.030

Carrivick, J. L., and M. W. SSmith MW (2019),. Fluvial and aquatic applications of Structure from Motion photogrammetry and unmanned aerial vehicle/drone technology, Wiley Interdisciplinary Reviews: Water., 6(1), : e1328. DOI: , doi: 10.1002/wat2.1328.

Cloud Compare. 2019. CloudCompare 2.10.2 [software]. Accessed 30/7/2019.

Cullen, A. and , Frey, H. (1999). Probabilistic Techniques in Exposure Assessment. Plenum Publishing Co., 1st edition.

Delignette-Muller ML, Marie Laure, and, Christophe Dutang C. 2015. "fitdistrplus: An R package for fitting distributions." Journal of Statistical Software. 64.4 (2015): 1-34. DOI: 10.18637/jss.v064.i04.

Demarchi L, Bizzi S, Piégay H. 2016. Hierarchical Object-Based Mapping of Riverscape Units and in-Stream Mesohabitats Using LiDAR and VHR Imagery. Remote Sensing. 8 : 97.

ESRI. 2014. ArcGIS 10.2.2.3552 for Desktop. Accessed 30/7/2019.

Eltner, A., Kaiser, A., Castillo, C., Rock, G., Neugirg, F. and Abellán, A. (2016). Image-based surface reconstruction in geomorphometry–merits, limits and developments. *Earth Surface Dynamics*, *4*(2), p. : 359-389.

Flener, C., M. Vaaja M, A. Jaakkola A, A. Krooks A, H. Kaartinen H, A. Kukko A, E. Kasvi E, H. Hyyppä H, J. Hyyppä J, and P. Alho P. (2013),. Seamless Mapping of River Channels at High Resolution Using Mobile LiDAR and UAV-Photography,. Remote Sensing,. 5(12), : 6382-6407. DOI: 10.3390/rs5126382

Folk RL, Ward WC. 1957. Brazos River bar: a study in the significance of grain size parameters. Journal of Sedimentary Petrology. 27 : 3-26.

Fonstad MA, Dietrich JT, Courville BC, Jensen JL, Carbonneau PE. 2013. Topographic structure from motion: a new development in photogrammetric measurement. Earth Surface Processes and Landforms. 38 : 421-430. DOI: 10.1002/esp.3366

Gilvear D, Cecil J, Parsons H. 2000. Channel change and vegetation diversity on a low-angle alluvial fan, River Feshie, Scotland. Aquatic Conservation: Marine and Freshwater Ecosystems. 10 : 53-71.

Glennie C, Brooks B, Ericksen T, Hauser D, Hudnut K, Foster J, Avery J. 2013. Compact Multipurpose Mobile Laser Scanning System — Initial Tests and Results. Remote Sensing. 5 : 521.

Hamshaw Scott SD, Thomas Bryce TB, Rizzo DMM. RD, O'Neil-Dunne J, Frolik J, Dewoolkar MMJarlath ON-D, Jeff F, M. DM. 201. 2017. Quantifying streambank movement and topography using unmanned aircraft system photogrammetry with comparison to terrestrial laser scanning. River Research and Applications. 33 : 1354-1367. DOI: 10.1002/rra.3183

Heritage GL, Milan DJ. 2009. Terrestrial Laser Scanning of grain roughness in a gravel-bed river. Geomorphology. 113 : 4-11. DOI: 0.1016/j.geomorph.2009.03.021

Hexagon. 2017. Novatel Intertial Explorer [software]. Accessed 2/6/2017.

Hodge RA, Brasington J, Richards K. 2009a. Analysing laser-scanned digital terrain models of gravel bed surfaces: linking morphology to sediment transport processes and hydraulics. Sedimentology. 56 : 2024-2043. DOI: 10.1111/j.1365-3091.2009.01068.x

Hodge RA, Brasington J, Richards K. 2009b. In situ characterization of grain-scale fluvial morphology using Terrestrial Laser Scanning. Earth Surface Processes and Landforms. 34 : 954-968. DOI: 10.1002/esp.1780

Jafari, B., Khaloo, A, . and Lattanzi, D.,. 2017. Deformation tracking in 3D point clouds via statistical sampling of direct cloud-to-cloud distances. Journal of Nondestructive Evaluation. , 36(4), p. : 65. DOI: 10.1007/s10921-017-0444-2

Jalonen J, Järvelä J, Koivusalo H, Hyyppä H. 2014. Deriving Floodplain Topography and Vegetation Characteristics for Hydraulic Engineering Applications by Means of Terrestrial Laser Scanning. Journal of Hydraulic Engineering. DOI: 140. 10.1061/(ASCE)HY.1943-7900.0000928

James MR, Robson S, D'oleire-Oltmanns S, Niethammer U. 2017. Optimising UAV topographic surveys processed with structure-from-motion: Ground control quality, quantity and bundle adjustment. Geomorphology. 280 : 51-66. DOI: 10.1016/j.geomorph.2016.11.021

James MR, Robson S. 2012. Straightforward reconstruction of 3D surfaces and topography with a camera: Accuracy and geoscience application. J. Geophys. Res. DOI: 117: F03017. 10.1029/2011jf002289

James MR, Robson S. 2014. Mitigating systematic error in topographic models derived from UAV and ground-based image networks. Earth Surface Processes and Landforms. 39 : 1413-1420. DOI: 10.1002/esp.3609

Jones AF, Brewer PA, Johnstone E, Macklin MG. 2007. High-resolution interpretative geomorphological mapping of river valley environments using airborne LiDAR data. Earth Surface Processes and Landforms. 32 : 1574-1592. DOI: 10.1002/esp.1505

Jung J, Yoon S, Ju S, Heo J. 2015. Development of Kinematic 3D Laser Scanning System for Indoor Mapping and As-Built BIM Using Constrained SLAM. Sensors. 15. DOI:10.3390/s151026430

Kasprak A, Brasington J, Hafen K, Williams RD, Wheaton JM. 2018. Modelling braided river morphodynamics using a particle travel length framework. Earth Surface Dynamics Discussion. DOI: 10.5194/esurf-2018-17

Kukko A, Kaartinen H, Hyyppä J, Chen Y. 2012. Multiplatform Mobile Laser Scanning: Usability and Performance. Sensors. 12 : 11712-11733.

Lague D, Brodu N, Leroux J. 2013. Accurate 3D comparison of complex topography with terrestrial laser scanner: Application to the Rangitikei canyon (N-Z). ISPRS Journal of Photogrammetry and Remote Sensing. 82 : 10-26. DOI: 10.1016/j.isprsjprs.2013.04.009

Lauterbach AH, Borrmann D, Heß R, Eck D, Schilling K, Nüchter A. 2015. Evaluation of a Backpack-Mounted 3D Mobile Scanning System. Remote Sensing. 7. DOI: 10.3390/rs71013753

Lee T. 2018. *Why experts believe cheaper, better lidar is right around the corner* [Online]. Arstechnica. Available: https://arstechnica.com/cars/2018/01/driving-around-without-a-driver-lidar-technology-explained/ [Accessed 1 August 2018].

Legleiter CJ. 2012. Remote measurement of river morphology via fusion of LiDAR topography and spectrally based bathymetry. Earth Surface Processes and Landforms. 37 : 499-518. DOI: 10.1002/esp.2262

Leica Geosystems. 2017. Pegasus: Manager [software]. Accessed 2/6/2017.

Leica Geosystems. 2019. Cyclone 9.3.2 [software]. Accessed 30/7/2019.

Liang, X., A. Kukko A, J. Hyyppä J, M. Lehtomäki M, J. Pyörälä J, X. Yu X, H. Kaartinen H, A. Jaakkola A, and Y., Wang Y. (2018),. In-situ measurements from mobile platforms: An emerging approach to address the old challenges associated with forest inventories,. ISPRS Journal of Photogrammetry and Remote Sensing., 143, : 97-107, doi: doi.org/. DOI:10.1016/j.isprsjprs.2018.04.019.

Liang, X., A. Kukko A, H. Kaartinen H, J. Hyyppä J, X. Yu X, A. Jaakkola A, and Y. Wang Y. (2014),. Possibilities of a Personal Laser Scanning System for Forest Mapping and Ecosystem Services,. Sensors,. 14(1), : 1228-1248. DOI: 10.3390/s140101228.

Lotsari, E., Y. Wang Y, H. Kaartinen H, A. Jaakkola A, A. Kukko A, M. Vaaja M, H. HHyyppä H, J. Hyyppä J, and P. Alho P. (2015),. Gravel transport by ice in a subarctic river from accurate laser scanning,. Geomorphology,. 246, : 113-122. DOI, doi: 10.1016/j.geomorph.2015.06.009.

Lotsari, E. SS., CM. Calle M, G. Benito G, A. Kukko A, H. Kaartinen H, J. Hyyppä J, H. Hyyppä H, and P. Alho P. (2018),. Topographical change caused by moderate and small floods in a gravel bed ephemeral river – a depth-averaged morphodynamic simulation approach,. Earth Surface Dynamics,. 6(1), : 163-185. DOI:, doi: 10.5194/esurf-6-163-2018.

Macdonald P. 2016. Change in Glen Feshie: environmental change in a dynamic Cairngorms landscape. *The Nature of Scotland.* Autumn / Winter 2106 ed. Inverness: Scottish Natural Heritage.

Manners R, Schmidt J, Wheaton JM. 2013. Multiscalar model for the determination of spatially explicit riparian vegetation roughness. Journal of Geophysical Research: Earth Surface. 118 : 65-83. DOI: 10.1029/2011JF002188

Milan DJ, Heritage GL, Hetherington D. 2007. Application of a 3D laser scanner in the assessment of erosion and deposition volumes and channel change in a proglacial river. Earth Surface Processes and Landforms. 32 : 1657-1674. DOI: 10.1002/esp.1592

Neverman, A. J., I. C. Fuller IC, J. N. Procter JN, and R. G. Death RG. (2019),. Terrestrial laser scanning and structure-from-motion photogrammetry concordance analysis for describing the surface layer of gravel beds,. Progress in Physical Geography: Earth and Environment. DOI:, doi: 10.1177/0309133318822966.

Oveland, I., M. Hauglin M, T. Gobakken T,, E. Næsset E, and I. Maalen-Johansen I. (2017),. Automatic Estimation of Tree Position and Stem Diameter Using a Moving Terrestrial Laser Scanner,. Remote Sensing., 9(4), : 350. DOI: 10.3390/rs9040350

Passalacqua P, Belmont P, Staley DM, Simley JD, Arrowsmith JR, Bode CA, Crosby C, Delong SB, Glenn NF, Kelly SA, Lague D, Sangireddy H, Schaffrath K, Tarboton DG, Wasklewicz T, Wheaton JM. 2015. Analyzing high resolution topography for advancing the understanding of mass and

energy transfer through landscapes: A review. Earth-Science Reviews. 148 : 174-193. DOI: 10.1016/j.earscirev.2015.05.012

Pasternack GB, Baig D, Weber MD, Brown RA. 2018. Hierarchically nested river landform sequences. Part 1: Theory. Earth Surface Processes and Landforms. DOI: 10.1002/esp.4411

Pearson E, Smith MW, Klaar MJ, Brown LE. 2017. Can high resolution 3D topographic surveys provide reliable grain size estimates in gravel bed rivers? Geomorphology. 293 : 143-155. DOI: 10.1016/j.geomorph.2017.05.015

Pix4D. 2019. Pix4Dmapper version 4.4.12 [software]. Accessed 30/7/2019.

R Core Team (2013). R: A language and environment for statistical computing. R Foundation for Statistical Computing, Vienna, Austria. URL http://www.R-project.org/. Accessed 30/7/2019.

Reid, H. E., R. D. WWilliams RD, G. J. Brierley GJ, S. E. Coleman SE, R. LLamb R, C. D. Rennie CD, and M. J. Tancock MJ. (2019),. Geomorphological effectiveness of floods to rework gravel bars: Insight from hyperscale topography and hydraulic modelling, Earth Surface Processes and Landforms,. 44 (2),: 595-613., doiDOI: 10.1002/esp.4521.

Riegl. 2017. RiScan Pro 2.0. [software]. Accessed 1/8/2017.

Rönnholm, P., X. Liang X, A. Kukko A, A. Jaakkola A, and J. Hyyppä J. (2016),. Quality analysis and correction of mobile backpack laser scanning data,. ISPRS Annals of Photogrammetry, Remote Sensing & Spatial Information Sciences. , 3(1),: 41-47,. DOI: doi: 10.5194/isprsannals-III-1-41-2016.

Rumsby BT, Brasington J, Langham JA, Mclelland SJ, Middleton R, Rollinson G. 2008. Monitoring and modelling particle and reach-scale morphological change in gravel-bed rivers: Applications and challenges. Geomorphology. 93 : 40-54. DOI: 10.1016/j.geomorph.2006.12.017

Sayama, T., K., Matsumoto K, Y. Kuwano Y, and K. Takara K. (2019),. Application of Backpack-Mounted Mobile Mapping System and Rainfall–Runoff–Inundation Model for Flash Flood Analysis,. Water. , 11(5), : 963, doi. DOI: 10.3390/w11050963.

Schneider JM, Rickenmann D, Turowski JM, Kirchner JW. 2015. Self-adjustment of stream bed roughness and flow velocity in a steep mountain channel. Water Resources Research. 51 : 7838-7859. DOI: 10.1002/2015WR016934

Smith MW, Carrivick JL, Quincey DJ. 2015. Structure from motion photogrammetry in physical geography. Progress in Physical Geography. 40 : 247-275. DOI: 10.1177/0309133315615805

Tamminga A, Hugenholtz C, Eaton B, Lapointe M. 2015. Hyperspatial Remote Sensing of Channel Reach Morphology and Hydraulic Fish Habitat Using an Unmanned Aerial Vehicle (UAV): A First Assessment in the Context of River Research and Management. River Research and Applications. 31 : 379-391. DOI: 10.1002/rra.2743

Tarolli P. 2014. High-resolution topography for understanding Earth surface processes: Opportunities and challenges. Geomorphology. 216 : 295-312. DOI: 10.1016/j.geomorph.2014.03.008

The Economist. 2016. A breakthrough in miniaturising lidars for autonomous driving. *The Economist.*

Vázquez-Tarrío D, Borgniet L, Liébault F, Recking A. 2017. Using UAS optical imagery and SfM photogrammetry to characterize the surface grain size of gravel bars in a braided river (Vénéon River, French Alps). Geomorphology. 285 : 94-105. DOI: 10.1016/j.geomorph.2017.01.039

Wang, Y., X. Liang X, C. Flener C, A. Kukko A, H. Kaartinen H, M. Kurkela M, M. Vaaja M, H. Hyyppä H, and P. Alho P. (2013),. 3D Modeling of Coarse Fluvial Sediments Based on Mobile Laser Scanning Data,. Remote Sensing., 5(9),: 4571-4592. DOI:10.3390/rs5094571

Wen, C., S. Pan S, C. Wang C, and J. Li J. (2016),. An Indoor Backpack System for 2-D and 3-D Mapping of Building Interiors, IEEE Geoscience and Remote Sensing Letters, . 13(7), : 992-996. , doiDOI: 10.1109/LGRS.2016.2558486.

Werritty A, Mcewen L (eds.) 1993. Glen feshie, London: Chapman and Hall.

Westoby MJ, Brasington J, Glasser NF, Hambrey MJ, Reynolds JM. 2012. 'Structure-from-Motion' photogrammetry: a low-cost, effective tool for geoscience applications. Geomorphology. 179 : 300-314. DOI: 10.1016/j.geomorph.2012.08.021

Westoby MJ, Dunning SA, Woodward J, Hein AS, Marrero SM, Winter K, Sugden DE. 2015. Sedimentological characterization of Antarctic moraines using UAVs and Structure-from-Motion photogrammetry. Journal of Glaciology. 61 : 1088-1102. DOI: 10.3189/2015JoG15J086

Wheaton JM, Brasington J, Darby SE, Kasprak A, Sear D, Vericat D. 2013. Morphodynamic signatures of braiding mechanisms as expressed through change in sediment storage in a gravel-bed river. Journal of Geophysical Research: Earth Surface. 118 : 759-779. DOI: 10.1002/jgrf.20060

Wheaton JM, Brasington J, Darby SE, Sear DA. 2010. Accounting for uncertainty in DEMs from repeat topographic surveys: improved sediment budgets. Earth Surface Processes and Landforms. 35 : 136-156. DOI: 10.1002/esp.1886

Williams RD, Brasington J, Hicks M, Measures R, Rennie CD, Vericat D. 2013. Hydraulic validation of two-dimensional simulations of braided river flow with spatially continuous aDcp data. Water Resources Research. 49 : 5183-5205. DOI: 10.1002/wrcr.20391

Williams RD, Brasington J, Vericat D, Hicks DM. 2014. Hyperscale terrain modelling of braided rivers: fusing mobile terrestrial laser scanning and optical bathymetric mapping. Earth Surface Processes and Landforms. 39 : 167-183. DOI: 10.1002/esp.3437

Williams RD, Measures R, Hicks DM, Brasington J. 2016. Assessment of a numerical model to reproduce event-scale erosion and deposition distributions in a braided river. Water Resources Research. 52 : 6621-6642. DOI: 10.1002/2015WR018491

Williams RD, Rennie CR, Brasington J, Hicks DM, Vericat D. 2015. Within-event spatially distributed bed material transport: linking apparent bedload velocity to morphological change. Journal of Geophysical Research: Earth Surface. 120 : 604-622. DOI: 10.1002/2014JF003346

Wolman MG. 1954. A method of sampling coarse bed material. Transactions of the American Geophysical Union. 35 : 951-956.

Woodget AS, Austrums R, Maddock IP, Habit E. 2017. Drones and digital photogrammetry: from classifications to continuums for monitoring river habitat and hydromorphology. Wiley Interdisciplinary Reviews: Water. 4 : e1222. DOI: 10.1002/wat2.1222

Acknowledgements

RTK-GNSS equipment were loaned through NERC Geophysical Equipment Facility (GEF) loan 1084; staff at NERC GEF are thanked for their technical assistance. We also thank Kenny Roberts, Runying Liu, Laura Strachan, Yebing Wang and Lichao Yu for field assistance; Leica Geosystems; Craig McDonnell for remote sensing technical assistance; the Glen Feshie Estate for enabling access to the study site; and two anonymous reviewers for their constructive comments.

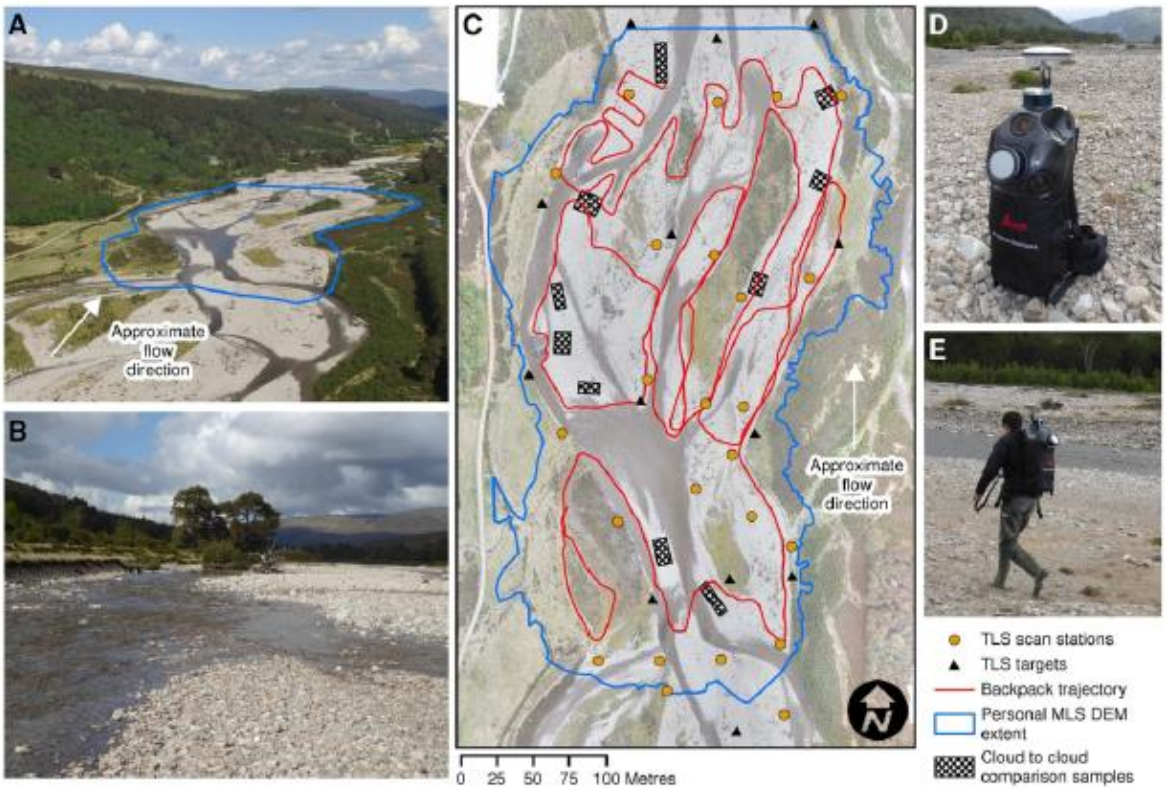

Figure 1. (a) Oblique aerial photograph of the River Feshie study site, Scotland. (b) Sediment example. (c) Survey setup. The aerial orthoimage was produced by acquiring RGB images from a DJI Phantom 4 UAV, which were processed using SfM photogrammetry (Pix4D, 2019). Root Mean Square Errors (RMSE) in X and Y for the aerial image were 0.038 and 0.039 m respectively (from n= 31 check point targets); these errors are sufficiently low to provide context for this figure. (d) The Leica Pegasus Backpack. (e) Acquiring data with personal MLS.

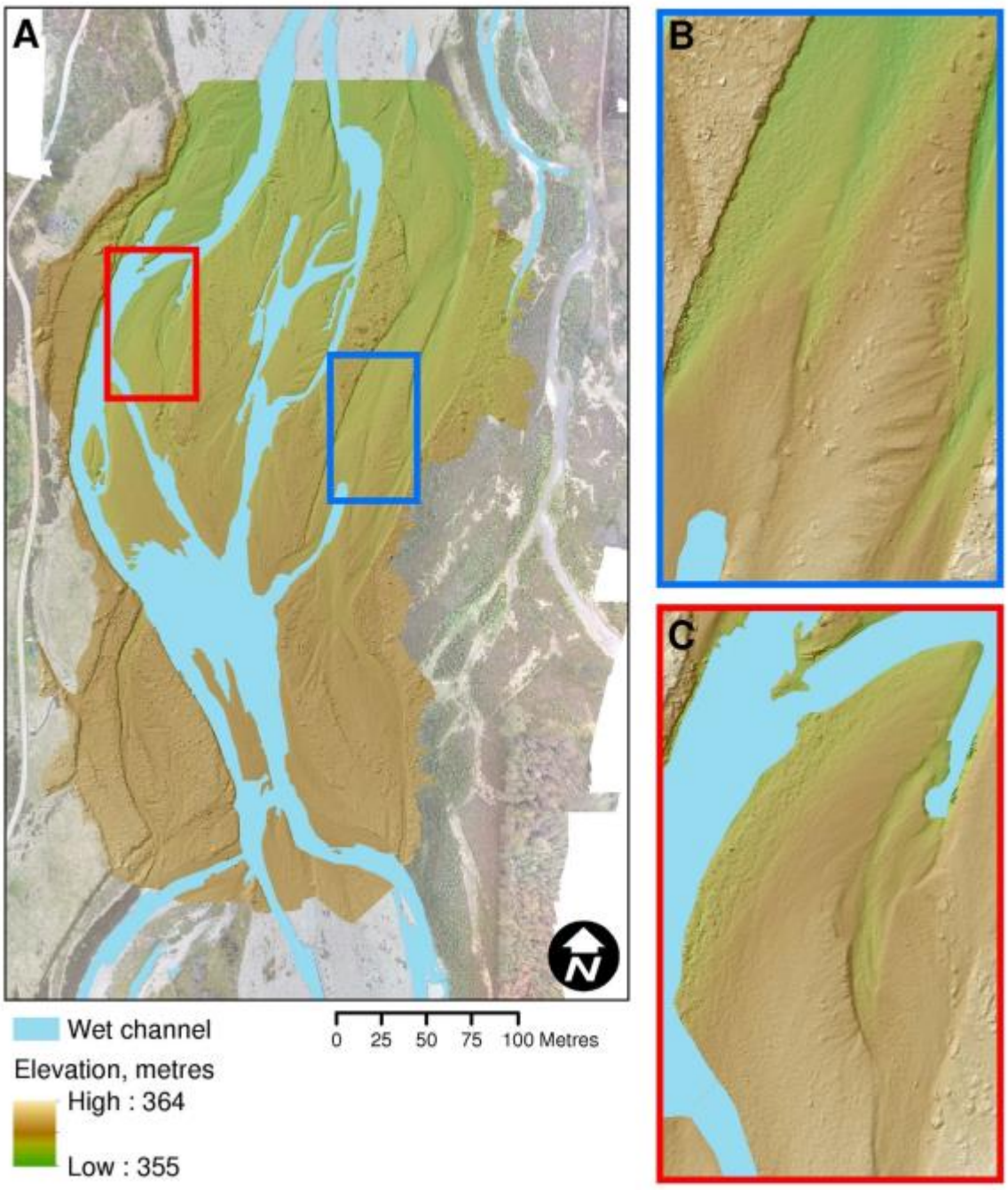

Figure 2. (A) 0.1 m resolution DEM of the study site produced from personal MLS observations. (B) and (C) Detail of diagonal bar topography; extent indicators are shown on (A).

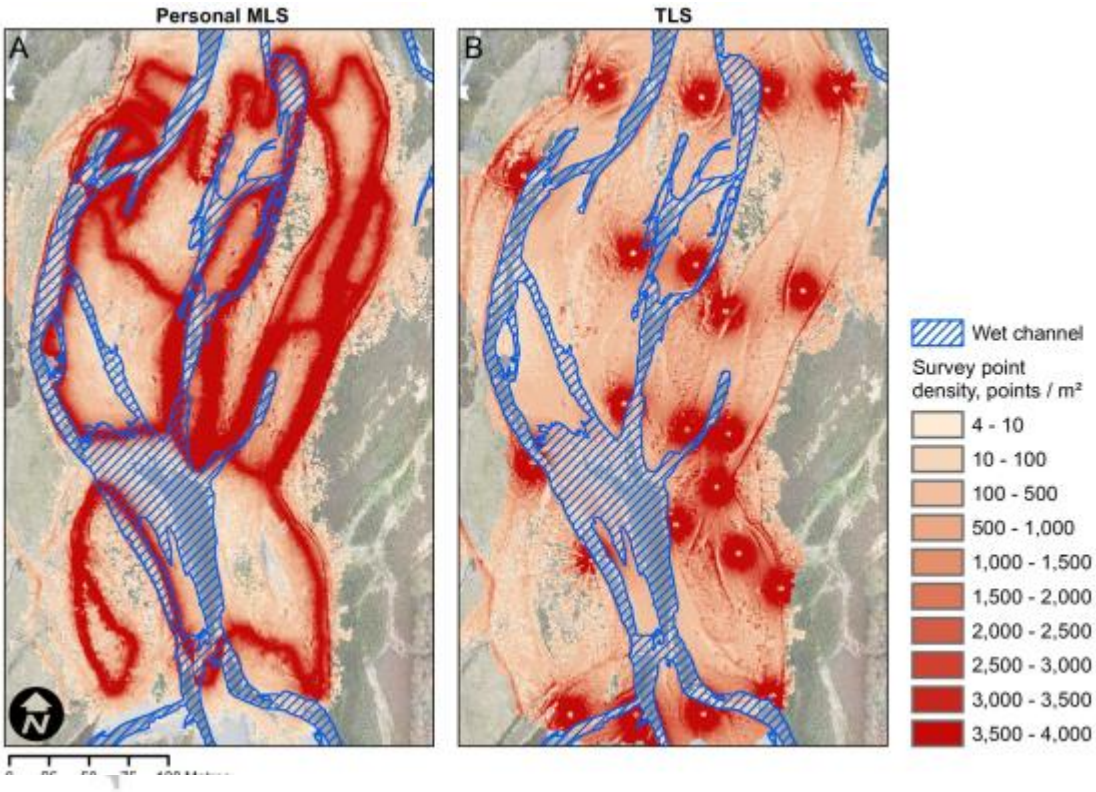

Figure 3. Point densities of the (a) personal MLS and (b) TLS point clouds produced after decimation to 0.02 m.

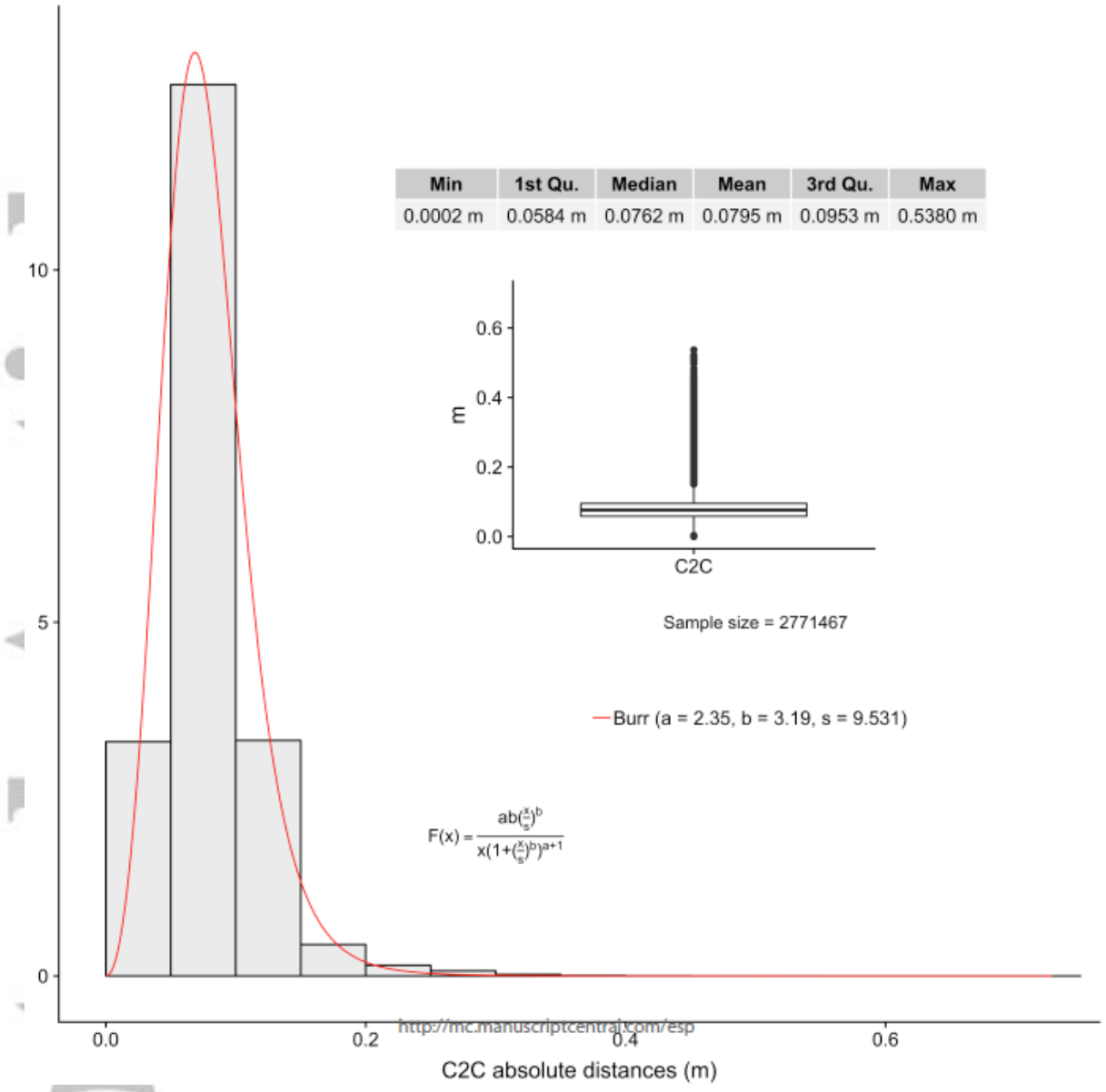

Figure 4. Distribution of C2C distances between personal MLS and TLS point clouds for the 10 sampled areas (shown in Figure 1c). The calculated C2C distances follow a sharply decreasing Burr distribution (a=2.35 b=3.19, rate parameter s = 9.53). The distribution was chosen after graphical and Goodness of fit criteria comparisons with another three candidate right-tail distributions (Weibull, gamma and log-normal; see Supplementary Material).

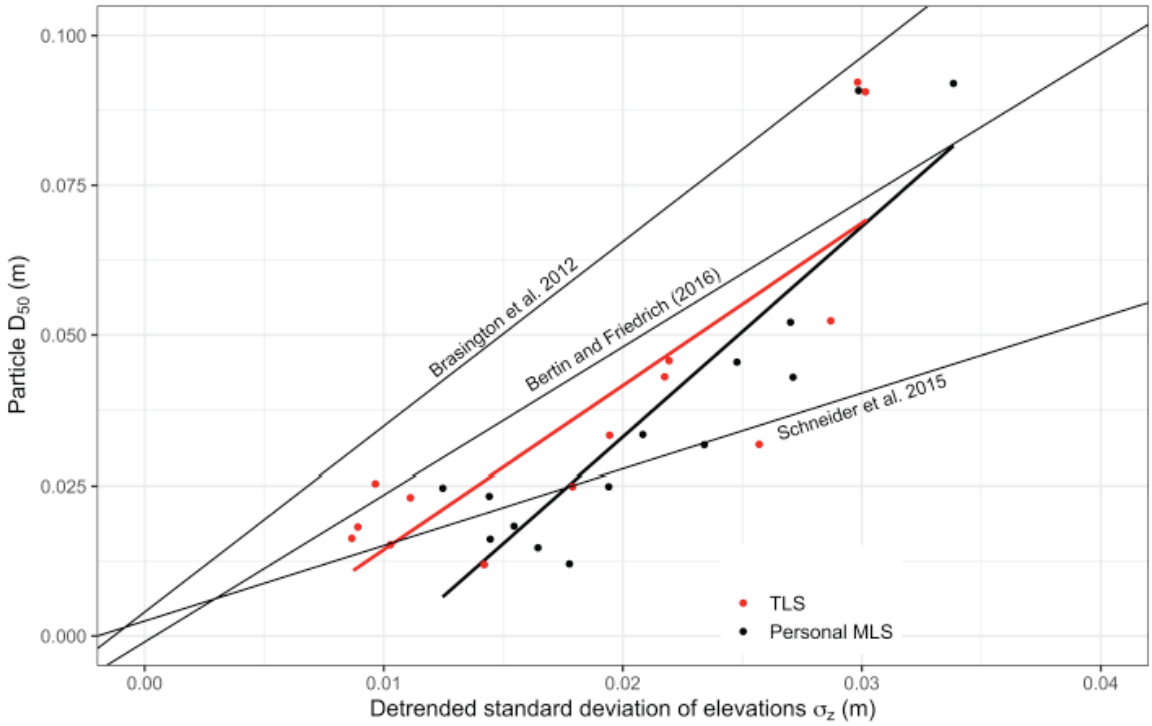

Figure 5. Comparison of D_{50}-σ_z relationships for personal MLS and TLS. The relationships derived in this study are compared to Brasington et al. (2012), Berlin and Friedlilch (2016) and Schneider et al. (2015). These three studies are analysed in Pearson et al.'s (2017) comparison of relationships and all have an R^2 goodness of fit > 0.9.

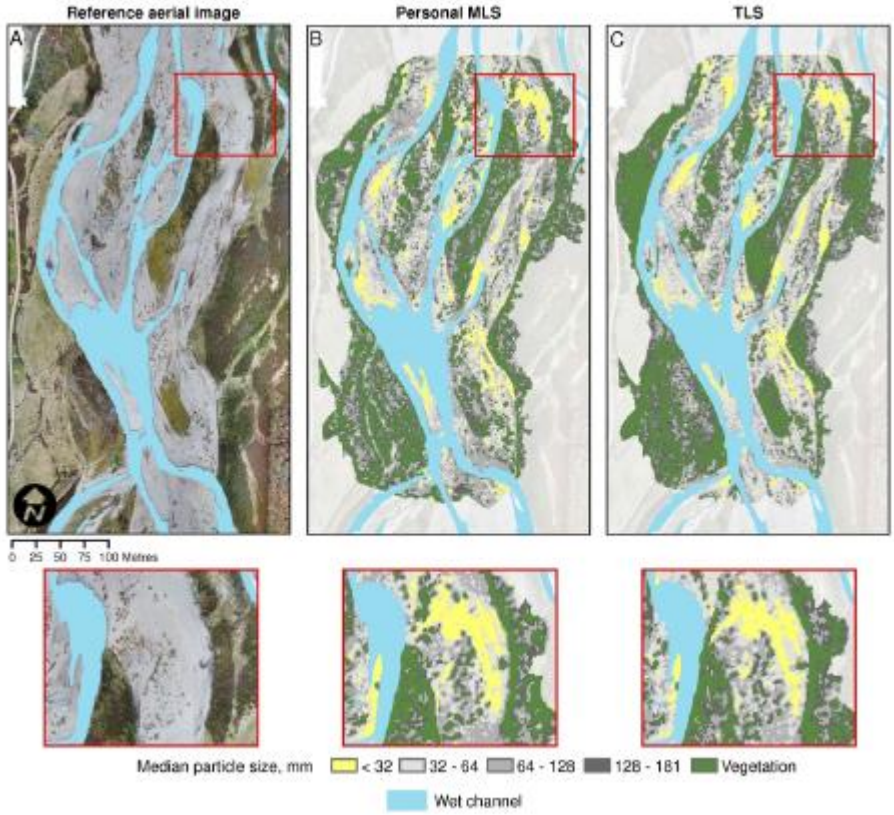

Figure 6. Reference aerial image (a) and maps of surface sedimentology derived from the relationships between particle D_{50} and detrended standard deviation of elevations, σ_z, for (b) personal MLS and (c) TLS.

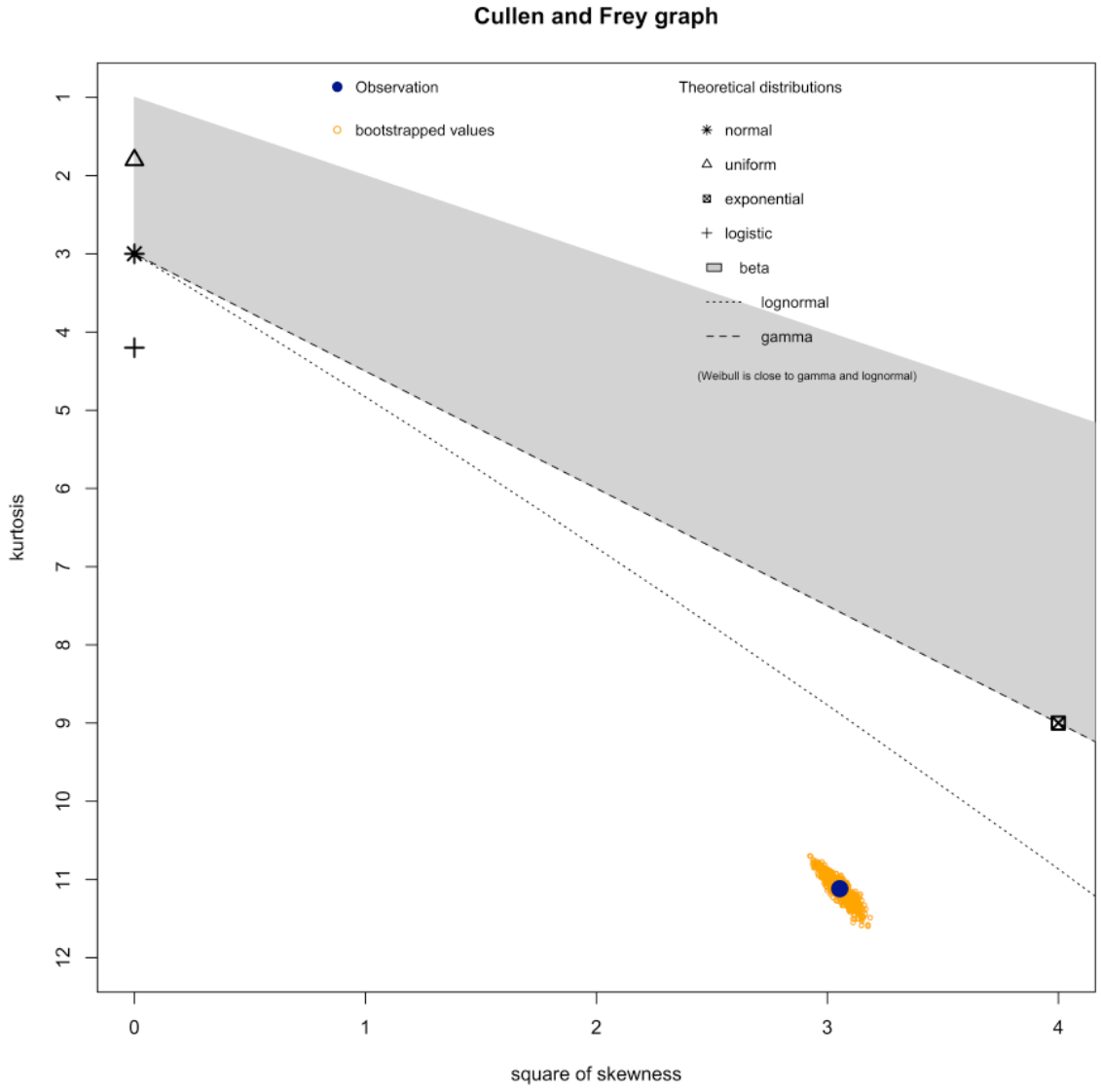

Figure S1: Cullen and Frey diagram for the identification of candidate distributions (MLS – TLS C2C distances, 10 sampled areas). The skewness vs kurtosis relationship (blue dot), indicates a right tail distribution as a candidate, which is not necessarily close to traditionally considered 2 parameter distributions (Weibull, gamma, log-normal). The 100 bootstrapped values (orange), indicate that the candidate distribution is relatively stable for the scale of the data.

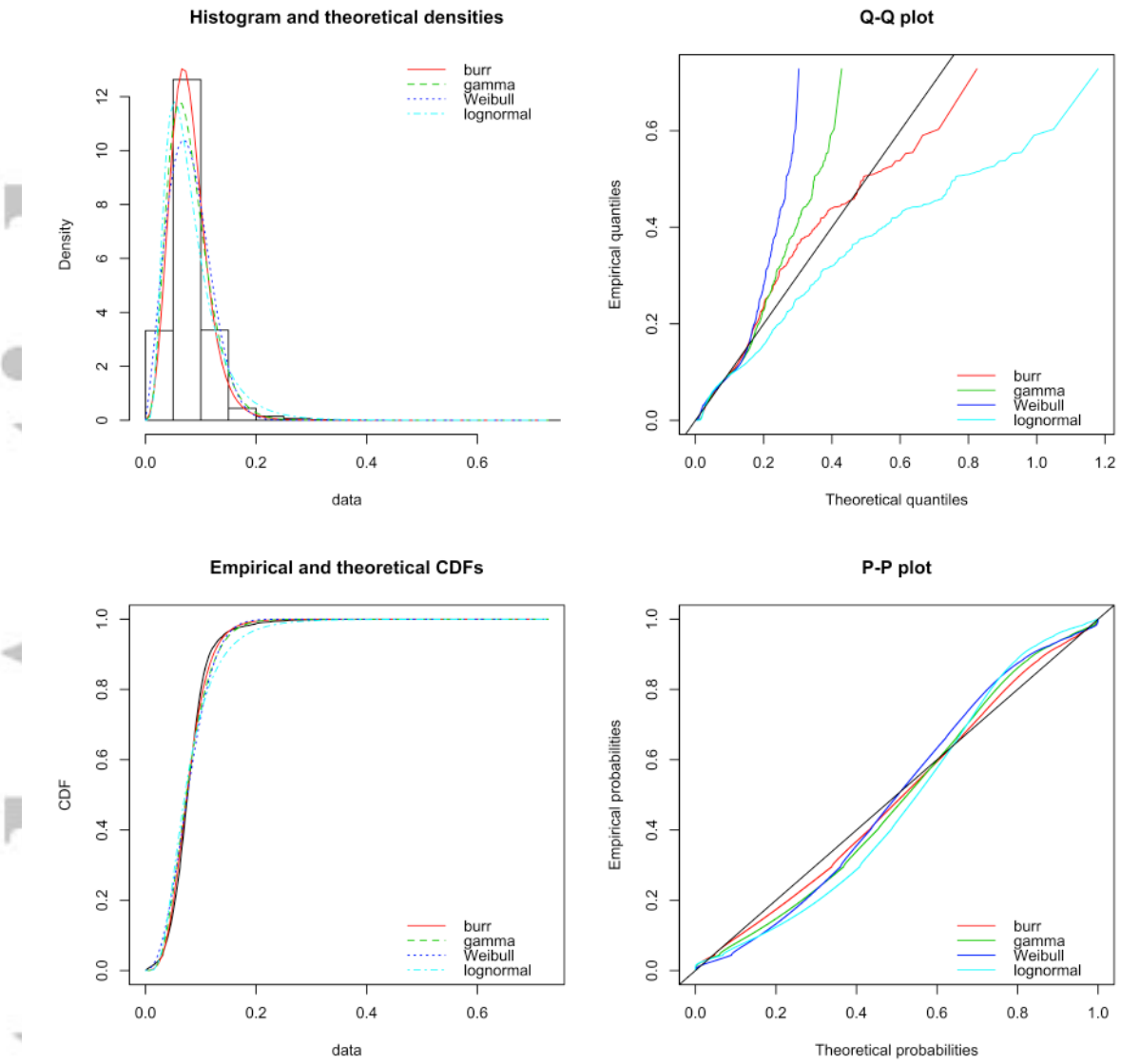

Figure S2: Graphical comparison between candidate distributions (MLS – TLS C2C distances, 10 sampled areas). None of the four tested distributions (Burr, Weibull, gamma and Log-normal) captures well the tails of the histogram (Q-Q plot), however the Burr distribution is the most representative of the four. The median values are better captured (P-P plot) with the Burr distribution outperforming again all the candidates. Finally, the Histogram and CDF diagrams indicate that the Burr distribution follows closer the empirical values.

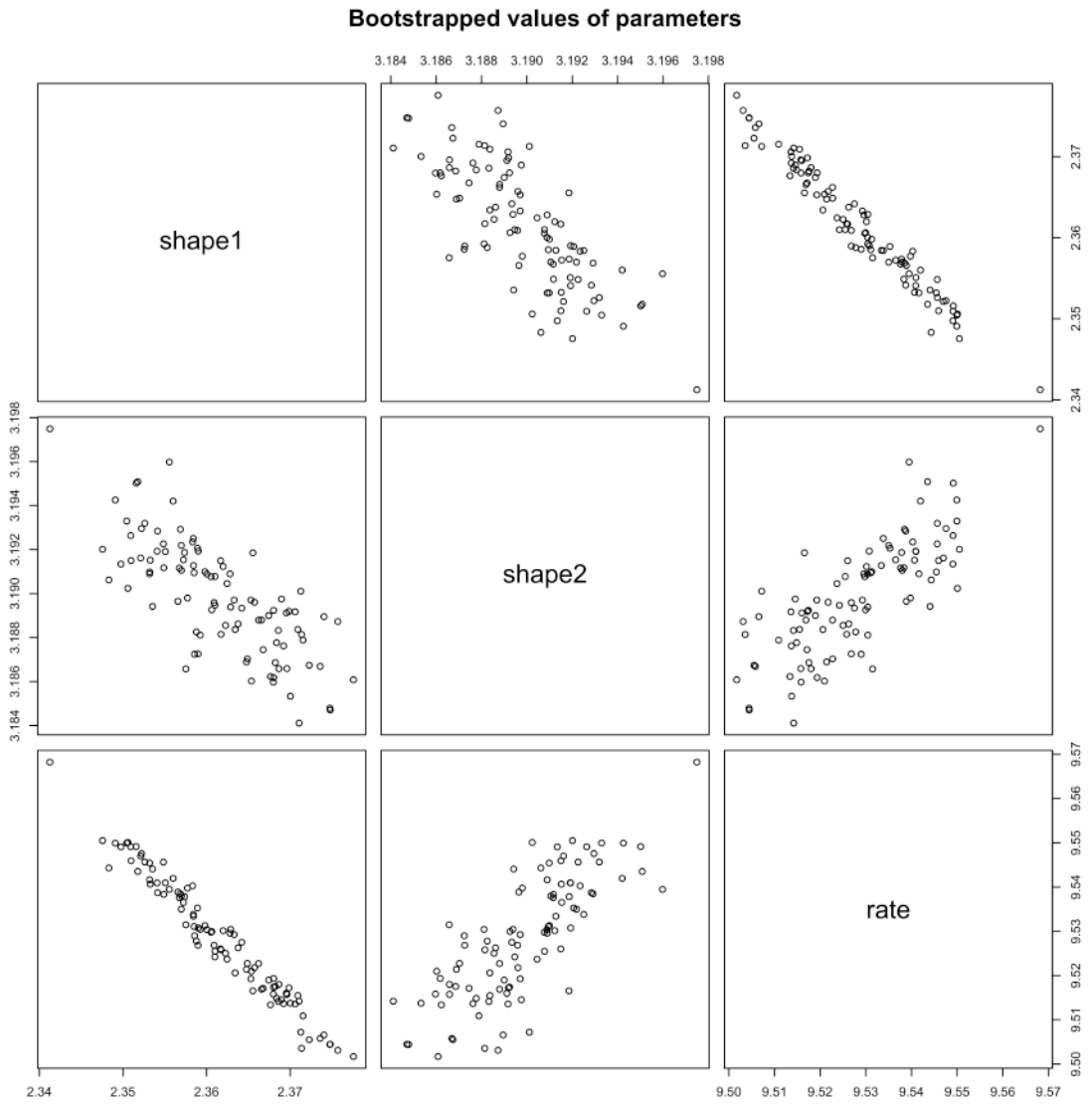

Figure S3: Stability of the chosen Burr distribution. 100 bootstrapped parameters were cross-compared, revealing a range of 0.04 for the a (shape1), 0.015 for the b (shape2) and 0.08 for s (rate) parameters. The differences are marginal, indicating good stability of the selected model. Within this marginal variance, there is structural correlation between the model parameters which can explain for the relatively poor fitting of the tails of the empirical distribution (when compared to the capture of the median values, Figure S2).

Table 1. Error analysis for positions of six targets surveyed with personal MLS. Point cloud positions are compared to target positions surveyed using GNSS-static observations. See Williams et al. (2014) for error formulae.

Error metric	**X, m**	**Y, m**	**Z, m**	**3D, m**
Mean Error (ME)	-0.025	-0.014	0.051	0.071
Standard Deviation Error (SDE)	0.038	0.019	0.028	0.026
Mean Absolute Error (MAE)	0.035	0.015	0.051	0.071
Root Mean Square Error (RMSE)	0.043	0.023	0.057	0.075

Table 2. Elevation error analysis for 107 RTK-GNSS check points compared to 0.1 m resolution personal MLS and TLS DEMs.

Error metric	**TLS, m**	**Personal MLS, m**
Mean Error (ME)	-0.025	-0.014
Standard Deviation Error (SDE)	0.038	0.019
Mean Absolute Error (MAE)	0.035	0.015
Root Mean Square Error (RMSE)	0.043	0.023

Table 3. Comparison between deployment challenges, data products and relative costs for three geoscientist operated topographic survey techniques.

Survey technique		**SfM photogrammetry**	**TLS**	**Personal MLS**
Deployment and processing challenges	**Field acquisition conditions**	Dry, low wind, sufficient daylight, flight permissions	Dry, low wind	All weather
	Field logistics	Target placement	Scan station locations	Sight lines from navigable terrain
	Data post-processing	Computational power, systematic error, point cloud filtering and editing	Point cloud filtering and editing	Point cloud filtering and editing
Data products	**Bathymetry**	Potential for reconstruction	Usually not water penetrating	Not water penetrating
	Point cloud product	Dense, evenly distributed	Dense, variable distribution	Dense, variable distribution
	Accuracy	Vertical range dependent	Planimetric range dependent	Planimetric range dependent
Relative costs	**Hardware and software**	Low	Medium	High
	Field logistics	Medium	High	Low
	Post processing	High	Medium	Medium

Table S1. Goodness fit criteria for the tested C2C distributions. AIC and BIC are from Akaike's and Bayesian Information Criteria.

Type of distribution	**Log-likelihood**	**AIC**	**BIC**
Weibull	5366993	-10733982	-10733956
Gamma	5394526	-10789048	-10789022
Log- normal	5040900	-10081797	-10081771
Burr	**5529989**	**-11059972**	**-11059934**

Three-dimensional reconstruction of fluvial surface sedimentology and topography using personal mobile laser scanning

Richard David Williams, Marie-Lou Lamy, Georgios Maniatis, Eilidh Stott

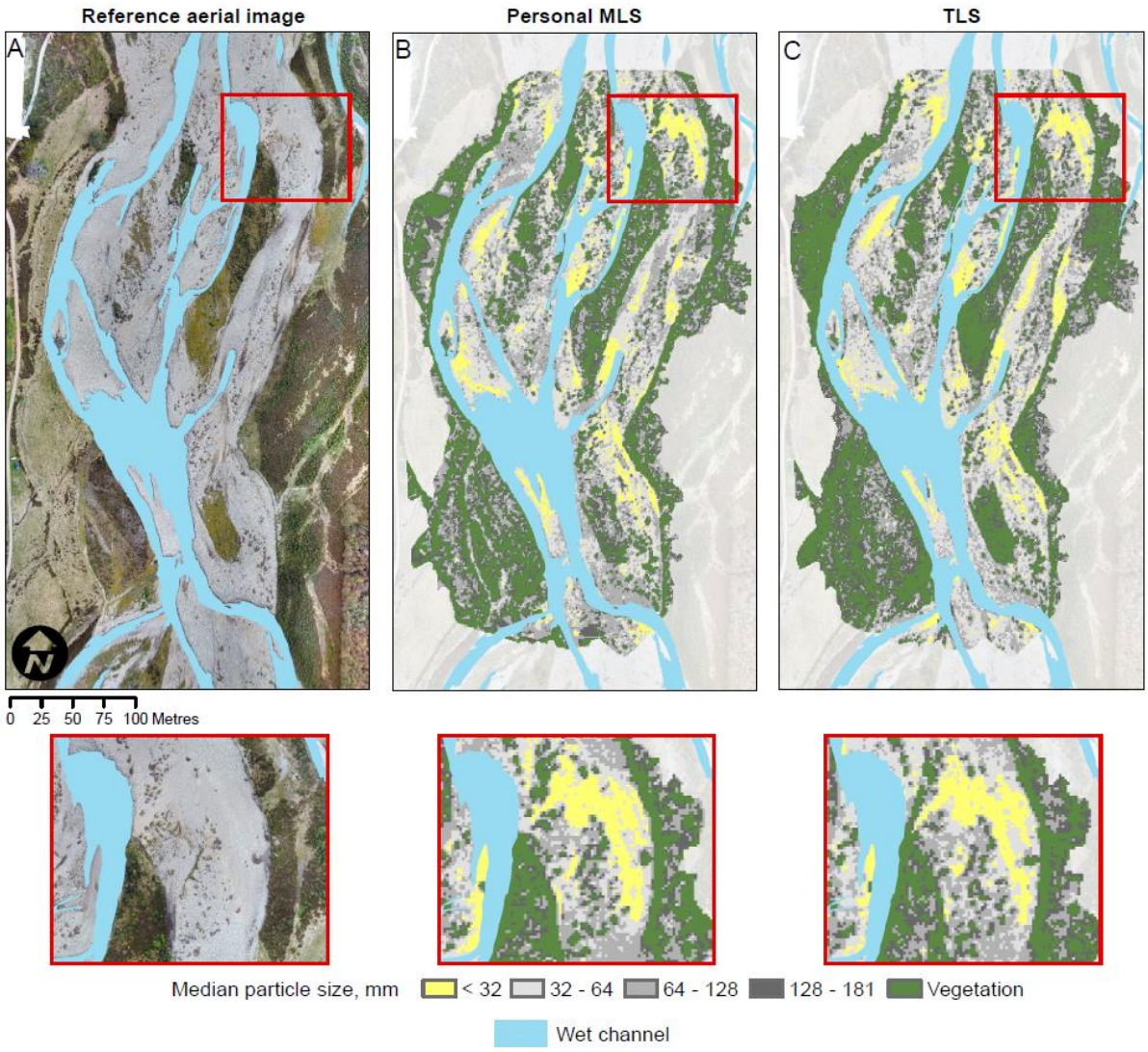

This investigation compares a personal mobile laser scanning (MLS) survey using a Leica Pegasus Backpack that integrates Velodyne Puck VLP-16 sensors, and a multi-station Terrestrial Laser Scanning (TLS) survey. Independent check points and a cloud-to-cloud comparison indicated that personal MLS had similar vertical errors to static TLS. Analysis of wearable laser scanning point cloud variability enabled the mapping of surface sedimentology. Where terrain is navigable by foot, wearable laser scanning enables rapid acquisition of point cloud data.